Available online at www.sciencedirect.com
SCIENCE DIRECT®
Journal of Sound and Vibration 281 (2005) 357–373
JOURNAL OF SOUND AND VIBRATION
www.elsevier.com/locate/jsvi

Divergence and flutter instability of elastic specially orthotropic plates subject to follower forces

Gopal Jayaraman[a], Allan Struthers[b,*]

[a]*Mechanical Engineering, Michigan Technological University, 1400 Townsend Drive, Houghton, MI 49931-1295, USA*
[b]*Department of Mathematical Sciences, Michigan Technological University, 1400 Townsend Drive, Houghton, MI 49931-1295, USA*

Received 2 June 2003; accepted 26 January 2004
Available online 5 October 2004

Abstract

Divergence and flutter instabilities of a rectangular, specially orthotropic plate (simply supported on a pair of opposite sides) subject to follower forces are computationally analyzed. The effects of the tangential follower parameter (η), aspect ratio (λ), boundary condition (on the side opposite the loaded edge), and material orthotropy on the magnitude of the critical load and the mode (divergence or flutter) of instability are detailed. For the three boundary conditions considered (built in, simply supported, and free free—for the side opposite the loaded edge) and given material orthotropy, the λ–η plane is divided into regions corresponding to different governing instabilities. Both the number and size of these regions depend strongly upon the boundary condition considered as does the governing instability. For a given boundary condition the configuration of the stability regions is independent of material orthotropy. Material orthotropy affects only the buckling loads corresponding to the instabilities and the size of the regions.

1. Introduction

The high strength-to-weight ratio of fiber-reinforced composites is making orthotropic plate structures increasingly common in weight-sensitive applications such as aeronautics, automotive design, offshore structures, and biomedical devices. The reduced thickness, made possible by the

*Corresponding author. Tel.: +1-906-487-2068; fax: +1-906-487-3133.
E-mail address: struther@mtu.edu (A. Struthers).

0022-460X/$ - see front matter © 2004 Elsevier Ltd. All rights reserved.
doi:10.1016/j.jsv.2004.01.033

high strength of these materials, makes the structural stability (both strength and buckling mode) of orthotropic plates an important design consideration for numerous industries. However, the elastic stability analysis of rectangular plates has focused mainly on the isotropic materials and conservative loads appropriate to heavy plates composed of traditional materials rather than the anisotropic materials and non-conservative loads appropriate to modern lighter plates. The influence of follower (or sub-follower forces) on buckling for composite plates has not been extensively analyzed. Most existing studies have either simply compared perfect follower loads to conservative loads or restricted attention to isotropic materials. In practice, most loads in complex structures are neither pure conservative nor pure follower and perhaps change as the structure ages. Generally, follower forces tend to increase the divergence buckling load and increase the likelihood of flutter. This paper systematically examines the effects of full/subtangential loading on the stability of orthotropic plates with a variety of widely employed boundary conditions. Stability studies of rectangular, orthotropic plates have focused on plates with boundary conditions typical of engineering analysis. In general, the loaded side is torque free but subject to a possibly subtangential load, the two sides perpendicular to the loaded side are simply supported, while the side opposite the loaded edge is either simply supported, built in, or satisfies a symmetry motivated boundary condition. Although any elastically constrained boundary condition could be studied with minor modifications of our procedure, we focus on the conventional boundary conditions.

Divergence instability studies of rectangular, orthotropic plates with conservative loading include: Wittrick [1] studied aspect ratio, boundary conditions, and material orthotropy effects using a correlation method; Shulesko [2] developed solutions using a reduction method; Brunille and Oyibo [3] provided generic buckling curves for specially orthotropic, rectangular plates; and several recent works [4–9] which examine effects of different boundary conditions, material orthotropy, and aspect ratio. Flutter instability studies of rectangular, isotropic plates with non-conservative loading include: Culkowski and Reismann [10] studied cantilevered plates with two follower forces; Leipholtz [11] and Leipholtz and Pfendt [12,13] investigated boundary condition effects; Adali [14] examined follower and in plane forces; Kumar and Srivasta [15] studied thin plates with two simply supported and two free edges with follower forces maintaining a specified angle of inclination on the free edges; Higuchi and Dowell [16] studied Poisson's ratio effects with free free boundary conditions while Reissner and Wan [17] considered similar effects for plates with two opposed simply supported and two opposed free edges with tangential follower forces on the free edges; Zuo and Shreyer [18] described divergence/flutter instability regions for simply supported plates with a combination of fixed and follower forces; and Farshad [19] examined biaxial subtangential loads. The only investigation of the interaction between orthotropy and follower loads is the recent paper by Kim and Kim [20] that treats the flutter instability of rectangular, cantilevered, orthotropic plates subject to follower forces.

The present investigation takes the position that for fault-tolerant design it is important to analyze structures for subtangential loads and examines the divergence/flutter instability regions for rectangular, specially orthotropic plates as the load changes from a conservative to a follower force. Since the buckling mode is a significant design criteria, the dependence of the instability regions on the aspect ratio, boundary conditions, and the generalized rigidity ratio quantifying material orthotropy are also studied.

2. Solution technique

We generally follow the development and notation of Zuo and Shreyer [18].

2.1. Governing equations

The thin, uniform, specially orthotropic plate, shown in Fig. 1, with mid plane coordinates x and y parallel to the material elastic symmetry axes is simply supported along the edges $x = 0$ and $x = a$ with a follower force N_y at the free edge $y = b/2$. Three different boundary conditions—simply supported (SS), built in (BI), and free free (FF)—are considered along the remaining edge $y = -b/2$. With $w(x, y, t)$ the lateral deflection at time t and coordinates (x, y), the bending

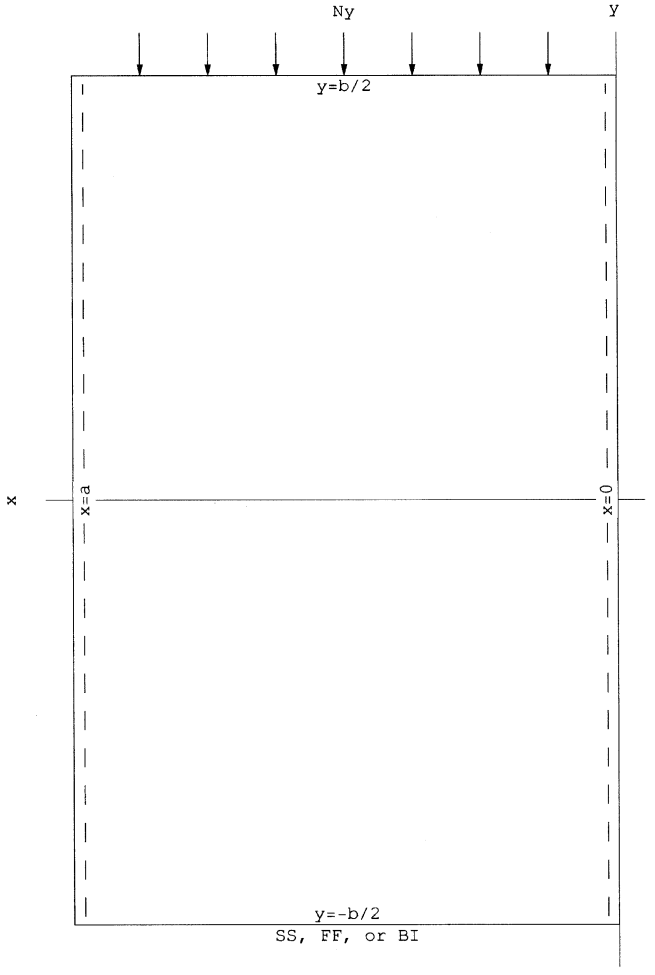

Fig. 1. Plate geometry and boundary conditions.

moments (M_x and M_y), twisting moment (M_{xy}), and shear forces (V_x and V_y) per unit length are

$$M_x = D_{11}\frac{\partial^2 w}{\partial x^2} + D_{12}\frac{\partial^2 w}{\partial y^2}, \quad M_y = D_{12}\frac{\partial^2 w}{\partial x^2} + D_{22}\frac{\partial^2 w}{\partial y^2},$$

$$M_{xy} = 2D_{66}\frac{\partial^2 w}{\partial x \partial y}, \quad v_x = -\frac{\partial M_x}{\partial x} - 2\frac{\partial M_{xy}}{\partial y}, \quad v_y = -\frac{\partial M_y}{\partial y} - 2\frac{\partial M_{xy}}{\partial x}, \tag{1}$$

where D_{ij} are the elastic constants of the plate. Balance of angular momentum [1] (with ρ the plate density) is

$$\frac{\partial^2 M_x}{\partial x^2} + 2\frac{\partial^2 M_{xy}}{\partial x \partial y} + \frac{\partial^2 M_y}{\partial y^2} + N_y\frac{\partial^2 w}{\partial y^2} + \rho\frac{\partial^2 w}{\partial t^2} = 0. \tag{2}$$

Substituting Eq. (1) into Eq. (2) gives the governing equilibrium equation for the orthotropic plate

$$D_{11}\frac{\partial^4 w}{\partial x^4} + 2(D_{12} + 2D_{66})\frac{\partial^4 w}{\partial x^2 \partial y^2} + D_{22}\frac{\partial^4 w}{\partial y^4} + N_y\frac{\partial^2 w}{\partial y^2} + \rho\frac{\partial^2 w}{\partial t^2} = 0. \tag{3}$$

Introducing the scaled coordinates x_0 and y_0 in addition to the scaled plate dimensions a_0 and b_0 (see for example Ref. [3]),

$$x = \sqrt{D_{11}^4}x_0 \quad \text{and} \quad y = \sqrt{D_{22}^4}y_0, \quad a = \sqrt{D_{11}^4}a_0 \quad \text{and} \quad b = \sqrt{D_{22}^4}b_0 \tag{4}$$

and defining the generalized rigidity ratio D^* and generalized Poisson's ratio ε by

$$D^* = \frac{D_{12} + 2D_{66}}{\sqrt{D_{11}D_{22}}}, \quad \varepsilon = \frac{D_{12}}{D_{12} + 2D_{66}} \tag{5}$$

transforms Eq. (3) to

$$\frac{\partial^4 w}{\partial x_0^4} + 2D^*\frac{\partial^4 w}{\partial x_0^2 \partial y_0^2} + \frac{\partial^4 w}{\partial y_0^4} + k\left(\frac{\pi}{a_0}\right)^2\frac{\partial^2 w}{\partial y_0^2} + \rho\frac{\partial^2 w}{\partial t^2} = 0, \tag{6}$$

where the affine plate buckling coefficient is the scaled load

$$k = \frac{N_y}{\sqrt{D_{22}}}\left(\frac{a_0}{\pi}\right)^2. \tag{7}$$

The simply supported boundary conditions at $x = 0$ and $x = a$ (or equivalently $x_0 = 0$ and $x_0 = a_0$) are

$$w(0, y, t) = w(a, y, t) = 0, \quad M_x(0, y, t) = M_x(a, y, t) = 0. \tag{8}$$

We write $w_0(x_0, y_0, t)$ for the displacement as a function of the scaled variables (4) and assume the form

$$w_0(x_0, y_0, t) = \sin(m\pi x_0/a_0)\, Y(y_0)e^{i\Omega t}. \tag{9}$$

This form, which automatically satisfies the simply supported ($w = 0$ and $M_x = 0$) boundary conditions at $x_0 = 0$ and $x_0 = a_0$, represents a steady-state vibration with frequency Ω and m half-waves in the x direction. The Levy form (9), which can be derived from a separation of variables argument, satisfies the governing partial differential equation (6) if Y satisfies the ordinary

differential equation

$$\frac{\mathrm{d}^4 Y}{\mathrm{d}y_0^4} - \left(\frac{\pi}{a_0}\right)^2 (2m^2 D^* - k)\frac{\mathrm{d}^2 Y}{\mathrm{d}y_0^2} + \left(\frac{\pi}{a_0}\right)^4 \left(m^4 - \frac{\rho\Omega^2 a_0^4}{\pi^4}\right) Y = 0. \tag{10}$$

Substituting $\zeta = \pi y_0/a_0$ and writing $f(\pi y_0/a_0) = Y(y_0)$ transforms Eq. (10) to

$$\frac{\mathrm{d}^4 f}{\mathrm{d}\zeta^4} - (2m^2 D^* - k)\frac{\mathrm{d}^2 f}{\mathrm{d}\zeta^2} + (m^4 - \omega^2) f = 0, \tag{11}$$

where $\omega^2 = \rho\Omega^2(a_0/\pi)^4$. Finally, substituting Eq. (9) into Eq. (1) reduces the expressions for the bending moments and shear forces to

$$\begin{aligned}
M_x &= \sqrt{D_{11}}\mathrm{e}^{\mathrm{i}t\Omega}\left(\frac{\pi}{a_0}\right)^2 \sin\left(\frac{m\pi x_0}{a_0}\right)[\varepsilon D^* f''(\zeta) - m^2 f(\zeta)],\\
M_y &= \sqrt{D_{22}}\mathrm{e}^{\mathrm{i}t\Omega}\left(\frac{\pi}{a_0}\right)^2 \sin\left(\frac{m\pi x_0}{a_0}\right)[f''(\zeta) - m^2\varepsilon D^* f(\zeta)],\\
M_{xy} &= (D_{11}D_{22})^{1/4}\mathrm{e}^{\mathrm{i}t\Omega}\left(\frac{\pi}{a_0}\right)^2 \cos\left(\frac{m\pi x_0}{a_0}\right)[m(\varepsilon - 1)D^* f'(\zeta)],\\
V_x &= (D_{11})^{1/4}\mathrm{e}^{\mathrm{i}t\Omega}\left(\frac{\pi}{a_0}\right)^3 \cos\left(\frac{m\pi x_0}{a_0}\right)[m^3 f(\zeta) + (\varepsilon - 2)mD^* f''(\zeta)],\\
V_y &= (D_{22})^{1/4}\mathrm{e}^{\mathrm{i}t\Omega}\left(\frac{\pi}{a_0}\right)^3 \sin\left(\frac{m\pi x_0}{a_0}\right)[m^2(\varepsilon - 2)D^* f'(\zeta) - f'''(\zeta)].
\end{aligned} \tag{12}$$

2.2. Boundary conditions

The explicit expressions (12) for the bending moments and shear forces show the Levy form (9) automatically satisfies simply supported boundary conditions at $x = 0$ and $x = a$. At $y = b/2$ the shear force must balance the applied follower load N_y and the bending moment is zero. The follower force and bending moment conditions at $y = b/2$ are

$$V_y = \eta N_y \,\mathrm{d}w/\mathrm{d}y, \quad M_y = 0, \tag{13}$$

where η is a parameter interpolating between the conservative force $\eta = 1$ and the follower force $\eta = 0$. Substituting expressions (12) for the shear force and bending moment into Eq. (13) gives

$$0 = f'''(\lambda/2) - (m^2(2 - \varepsilon)D^* - \eta k)f'(\lambda/2), \quad 0 = f''(\lambda/2) - m^2\varepsilon D^* f(\lambda/2), \tag{14}$$

where the scaled plate aspect ratio λ is

$$\lambda = \pi\frac{b_0}{a_0} = \pi\frac{b}{a}\left(\frac{D_{11}}{D_{22}}\right)^{1/4}. \tag{15}$$

Three different boundary conditions are considered at $y = -b/2$. For a built in (BI) end, $w = 0$ and $\mathrm{d}w/\mathrm{d}y = 0$ at $y = -b/2$. For a simply supported (SS) end $w = 0$ and $M_y = 0$ at $y = -b/2$. For a free free (FF) end with conservative loading ($\eta = 1$), $M_y = 0$ and $V_y = 0$ at $y = -b/2$.

These boundary conditions are the most common in practice and are physically realizable with FF, SS, and BI corresponding to increasingly stiff support structures. Expressions (9), (12) and (14) give the following boundary conditions for BI, SS, and FF:

$$\mathrm{BI} - \begin{cases} f(-\lambda/2) = 0, \\ f'(-\lambda/2) = 0; \end{cases} \tag{16}$$

$$\mathrm{SS} - \begin{cases} f(-\lambda/2) = 0, \\ f''(-\lambda/2) = 0; \end{cases} \tag{17}$$

$$\mathrm{FF} - \begin{cases} f''(-\lambda/2) - m^2 \varepsilon D^* f(-\lambda/2) = 0, \\ f'''(-\lambda/2) - (m^2(2-\varepsilon)D^* - k) f'(-\lambda/2) = 0. \end{cases} \tag{18}$$

To compare our results with Zuo and Schreyer [18] we follow their argument and decompose the FF boundary conditions into simpler even (EFF) and odd (OFF) free free boundary conditions applied at the midpoint $y = 0$ of the plate:

$$\mathrm{OFF} - \begin{cases} f(0) = 0, \\ f''(0) = 0; \end{cases} \tag{19}$$

$$\mathrm{EFF} - \begin{cases} f'(0) = 0, \\ f'''(0) = 0. \end{cases} \tag{20}$$

It should be noted that the OFF boundary conditions are (after an elementary scaling argument) the SS boundary conditions for a plate with aspect ratio $\lambda/2$.

2.3. Characteristic equation

The generic form of the general solution of the ordinary differential equation (11) is

$$f(\zeta) = C_1 \mathrm{e}^{\alpha_1 \zeta} + C_2 \mathrm{e}^{\alpha_2 \zeta} + C_3 \mathrm{e}^{\alpha_3 \zeta} + C_4 \mathrm{e}^{\alpha_4 \zeta}, \tag{21}$$

where α_1, α_2, α_3, and α_4 are the four generically distinct roots of the characteristic polynomial

$$\alpha^4 - (2m^2 D^* - k)\alpha^2 + (m^4 - \omega^2) = 0 \tag{22}$$

given by

$$\alpha = \pm(2m^2 D^* - k) \pm \sqrt{(k - 2m^2 D^*)^2 + 4(\omega^2 - m^2)}/\sqrt{2}. \tag{23}$$

The number and complexity of the boundary conditions considered in this paper negate the benefits exploited in Ref. [14] of rewriting solution (21) as explicitly real expression containing trigonometric and/or hyperbolic functions depending on the nature of the roots (23). The only drawback to our explicitly complex calculation is the unavoidable presence, due to numerical round off, of extremely small imaginary floating point values, which we simply discard, in our results.

Substituting Eq. (21) into the follower force condition (14) at $y = b/2$ (equivalently $\zeta = \lambda/2$) gives the two linear equations

$$a_1C_1 + a_2C_2 + a_3C_3 + a_4C_4 = 0, \quad b_1C_1 + b_2C_2 + b_3C_3 + b_4C_4 = 0 \tag{24}$$

for the constants C_1,C_2,C_3, and C_4 where the coefficients a_i and b_i are

$$a_i = (\alpha_i^2 - \varepsilon D^* m^2)\mathrm{e}^{\alpha_i\lambda/2}, \quad b_i = (\alpha_i^3 - \alpha_i[(2-\varepsilon)D^* m^2 - \eta k])\mathrm{e}^{\alpha_i\lambda/2}. \tag{25}$$

The BI and SS boundary conditions (16) and (17) at $y = -b/2$ (equivalently $\zeta = -\lambda/2$) give two additional linear equations

$$\mathrm{BI} - \begin{cases} \mathrm{e}^{-\alpha_1\lambda/2}C_1 + \mathrm{e}^{-\alpha_2\lambda/2}C_2 + \mathrm{e}^{-\alpha_3\lambda/2}C_3 + \mathrm{e}^{-\alpha_4\lambda/2}C_4 = 0, \\ \alpha_1\mathrm{e}^{-\alpha_1\lambda/2}C_1 + \alpha_2\mathrm{e}^{-\alpha_2\lambda/2}C_2 + \alpha_3\mathrm{e}^{-\alpha_3\lambda/2}C_3 + \alpha_4\mathrm{e}^{-\alpha_4\lambda/2}C_4 = 0; \end{cases} \tag{26}$$

$$\mathrm{SS} - \begin{cases} \mathrm{e}^{-\alpha_1\lambda/2}C_1 + \mathrm{e}^{-\alpha_2\lambda/2}C_2 + \mathrm{e}^{-\alpha_3\lambda/2}C_3 + \mathrm{e}^{-\alpha_4\lambda/2}C_4 = 0, \\ \alpha_1^2\mathrm{e}^{-\alpha_1\lambda/2}C_1 + \alpha_2^2\mathrm{e}^{-\alpha_2\lambda/2}C_2 + \alpha_3^2\mathrm{e}^{-\alpha_3\lambda/2}C_3 + \alpha_4^2\mathrm{e}^{-\alpha_4\lambda/2}C_4 = 0; \end{cases} \tag{27}$$

while the OFF and EFF boundary conditions at $y = 0$ (equivalently $\zeta = 0$) give the linear equations

$$\mathrm{OFF} - \begin{cases} C_1 + C_2 + C_3 + C_4 = 0, \\ \alpha_1^2C_1 + \alpha_2^2C_2 + \alpha_3^2C_3 + \alpha_4^2C_4 = 0; \end{cases} \tag{28}$$

$$\mathrm{EFF} - \begin{cases} \alpha_1C_1 + \alpha_2C_2 + \alpha_3C_3 + \alpha_4C_4 = 0, \\ \alpha_1^3C_1 + \alpha_2^3C_2 + \alpha_3^3C_3 + \alpha_4^3C_4 = 0 \end{cases} \tag{29}$$

for the constants C_1,C_2,C_3, and C_4. Each set of boundary conditions gives a matrix

$$A_{\mathrm{BI}} = \begin{pmatrix} \mathrm{e}^{-\alpha_1\lambda/2} & \mathrm{e}^{-\alpha_2\lambda/2} & \mathrm{e}^{-\alpha_3\lambda/2} & \mathrm{e}^{-\alpha_4\lambda/2} \\ \alpha_1\mathrm{e}^{-\alpha_1\lambda/2} & \alpha_2\mathrm{e}^{-\alpha_2\lambda/2} & \alpha_3\mathrm{e}^{-\alpha_3\lambda/2} & \alpha_4\mathrm{e}^{-\alpha_4\lambda/2} \\ a_1 & a_2 & a_3 & a_4 \\ b_1 & b_2 & b_3 & b_4 \end{pmatrix}, \tag{30}$$

$$A_{\mathrm{SS}} = \begin{pmatrix} \mathrm{e}^{-\alpha_1\lambda/2} & \mathrm{e}^{-\alpha_2\lambda/2} & \mathrm{e}^{-\alpha_3\lambda/2} & \mathrm{e}^{-\alpha_4\lambda/2} \\ \alpha_1^2\mathrm{e}^{-\alpha_1\lambda/2} & \alpha_2^2\mathrm{e}^{-\alpha_2\lambda/2} & \alpha_3^2\mathrm{e}^{-\alpha_3\lambda/2} & \alpha_4^2\mathrm{e}^{-\alpha_4\lambda/2} \\ a_1 & a_2 & a_3 & a_4 \\ b_1 & b_2 & b_3 & b_4 \end{pmatrix}, \tag{31}$$

$$A_{\mathrm{OFF}} = \begin{pmatrix} 1 & 1 & 1 & 1 \\ \alpha_1^2 & \alpha_2^2 & \alpha_3^2 & \alpha_4^2 \\ a_1 & a_2 & a_3 & a_4 \\ b_1 & b_2 & b_3 & b_4 \end{pmatrix}, \quad A_{\mathrm{EFF}} = \begin{pmatrix} \alpha_1 & \alpha_2 & \alpha_3 & \alpha_4 \\ \alpha_1^3 & \alpha_2^3 & \alpha_3^3 & \alpha_4^3 \\ a_1 & a_2 & a_3 & a_4 \\ b_1 & b_2 & b_3 & b_4 \end{pmatrix}. \tag{32,33}$$

For a matrix A chosen from Eqs. (30)–(33), substituting a coefficient vectors $\vec{C} = [C_1, C_2, C_3, C_4]$ satisfying

$$A\vec{C} = 0 \tag{34}$$

into Eq. (21) gives a solution of Eq. (11) satisfying the boundary conditions associated with the matrix. Non-trivial solutions to Eq. (34), which exist when the characteristic equation

$$\det(A) = 0 \tag{35}$$

is satisfied, indicate instability of the undisturbed equilibrium $w = 0$. The time dependence $e^{i\Omega t}$ of a non-trivial solution (where $\Omega = \pm\omega(\pi/a_0)1/\sqrt{\rho}$) determines the nature of the instability: if $\Omega = 0$ there is an adjacent static equilibrium; if $\Omega = \Omega_r + i\Omega_i$ with imaginary part $\Omega_i \neq 0$ then there is an exponentially growing disturbance. An adjacent static equilibrium indicates a divergence instability. An exponentially growing solution indicates a flutter instability.

2.4. Computational notes

Expressions (30)–(33) for the matrices A_{BI}, A_{SS}, A_{OFF} and A_{EFF} involve the material parameters ε and D^*, the mode number m, the frequency ω, the load k, the follower parameter η, and the affine aspect ratio λ. However, the follower parameter η, which is not involved in expression (23) for the roots α, appears only in the fourth row of each matrix. As a result, the characteristic equation (35) is linear in η for each of the four boundary conditions. Solving this linear equation gives a complicated but explicit expression of the form

$$\eta = F(k, \lambda, \omega, m, \varepsilon, D^*) \tag{36}$$

for the follower parameter satisfying Eq. (35). The explicit form of F depends on the boundary conditions.

2.4.1. Explicitly complex arithmetic

The explicitly complex computation of η described above has the significant advantage of combining five real computations (generated by five distinct forms for the roots of Eq. (22), [14]) into one complex computation. The only drawback is that although the η values given by Eq. (36) should be real, incomplete cancellation (in the complex floating point computation) leaves a small imaginary residue in the computed η. The insignificant (in the computations reported less than 10^{-12}) imaginary part is simply neglected.

2.4.2. Generic solutions

The generic solution form (21) is appropriate when Eq. (22) has four distinct roots. There are repeated roots of Eq. (22) if either

$$(\omega^2 - m^2) + (k/2 - m^2D^*)^2 = 0, \quad \text{or} \quad (\omega^2 - m^2) = 0. \tag{37}$$

The explicit form of the solution can be computed for either (or both) degeneracy. However, we do not need these degenerate forms. The simple solution is to avoid these non-generic cases by avoiding the specific frequency $\omega = m$ and the specific loads $k = 2m^2D^* \pm 2\sqrt{|\omega^2 - m^2|}$.

2.4.3. Explicit expression

Solving the characteristic equation (35) to give η as a function (36) of the remaining parameters avoids repeatedly solving the non-linear equation (35) for the buckling load k.

2.4.4. Non-physical values and singularities

Expressions (36) gives values for η outside the physical range $0 \leqslant \eta \leqslant 1$ for many parameter values and in addition the expressions are singular along various curves in the parameter space. This does not pose a problem. We simply disregard values of η outside the physical range $0 \leqslant \eta \leqslant 1$ and avoid interpolation in the η values.

2.4.5. Computational range

Eq. (35) would normally be solved for k. To exploit Eq. (36), k is considered as an independent variable. As a consequence, the computational range of k is restricted. Throughout the paper this maximum non-dimensionalized load is 12. Blank regions in figures imply that either no buckling load exists or that the non-dimensional buckling load exceeds 12.

2.4.6. Divergence loads

A value of k for which the plate exhibits a divergence instability is a divergence critical load. In other words, a divergence critical load is a solution of the characteristic equation (35) with frequency $\omega = 0$.

For a given boundary condition and specified m, ε, and D^* divergence, critical loads are computed by compiling η values—using the appropriate version of Eq. (36)—on a regular grid of more than a quarter of a million λ and k values with $0.5 \leqslant \lambda \leqslant 4$ and $0 < k \leqslant 12$. For each λ the smallest k value giving $\eta = 0.00, 0.01, \ldots$ up to $\eta = 1.00$ was computed (with piecewise linear interpolation in k) to generate a data set giving divergence critical loads as a function of λ and η. Values of λ and η for which no k value is found (either because no divergence critical load exists for the plate or because the divergence critical load exceeds 12) are flagged.

2.4.7. Flutter loads

A value of k for which the plate exhibits a flutter instability is a flutter critical load. The boundary of the flutter instability region is characterized by the marginally stable solutions of Eq. (35) with $\omega = \omega_r + \omega_i \mathrm{i}$ and $\omega_i = 0$. For most purposes the frequency ω_r is irrelevant and only the flutter stability boundary (the minimum flutter critical load k over all possible frequencies ω_r) is reported.

We continue to exploit the explicit expression (36) for the follower parameter by noting that

$$\eta = F(\hat{k}(\omega), \lambda, \omega, m, \varepsilon, D^*) \Rightarrow 0 = \frac{\partial F}{\partial k}\frac{\mathrm{d}\hat{k}}{\mathrm{d}\omega} + \frac{\partial F}{\partial \omega}. \tag{38}$$

As a result, at a local minimum of $\hat{k}(\omega)$, i.e. a flutter critical load on such a curve one has

$$\frac{\partial F}{\partial \omega} = 0. \tag{39}$$

For a given boundary condition and specified m, ε, and D^*, flutter critical loads are computed by compiling η values using Eq. (36) on a grid of more than 20 million λ, k and ω values with

$0.5 \leqslant \lambda \leqslant 4$ and $0 < k \leqslant 12$, and $0 \leqslant \omega \leqslant 10$. Differencing this data set in ω identifies solutions of Eq. (39) which gives $\{\eta, \omega\}$ pairs satisfying Eqs. (35) and (39). Flutter critical loads are extracted from these η values using the procedure described before for divergence critical loads. As before, values of λ and η at which no flutter critical load is found are flagged.

3. Mode shapes

Mode shapes are readily computed by substituting the constants C_1, C_2, C_3, C_4 from Eq. (34) back into Eq. (21). Complicated mode shapes can result. A fundamental mode shape has no inflection points.

4. Stability curves

The aim of this paper is to illustrate the effects of the boundary conditions BI, SS, FF defined in Eqs. (16)–(18), generalized rigidity ratio D^* defined in Eq. (5), scaled plate aspect ratio λ defined in Eq. (15), and follower parameter η on both flutter and divergence loads. We first focus on the boundary conditions. Then we examine the dependence of the divergence and flutter loads on λ. We conclude with the dependence on D^*. All subsequent computations and figures have fundamental transverse mode shape, $m = 1$. Higher order transverse mode shapes were found to give significantly greater critical loads.

4.1. Divergence and flutter load dependence on boundary conditions

Fig. 2 compares Built In (BI), Simply Supported (SS), Free-Free (Even—EFF and Odd—OFF) divergence and flutter loads for $0 \leqslant \eta \leqslant 1$ with aspect ratio $\lambda = 3.5$, material orthotropy $D^* = 1.0$, and $\varepsilon = 0.3$. The heavy curves are divergence loads while the light curves are flutter loads. We

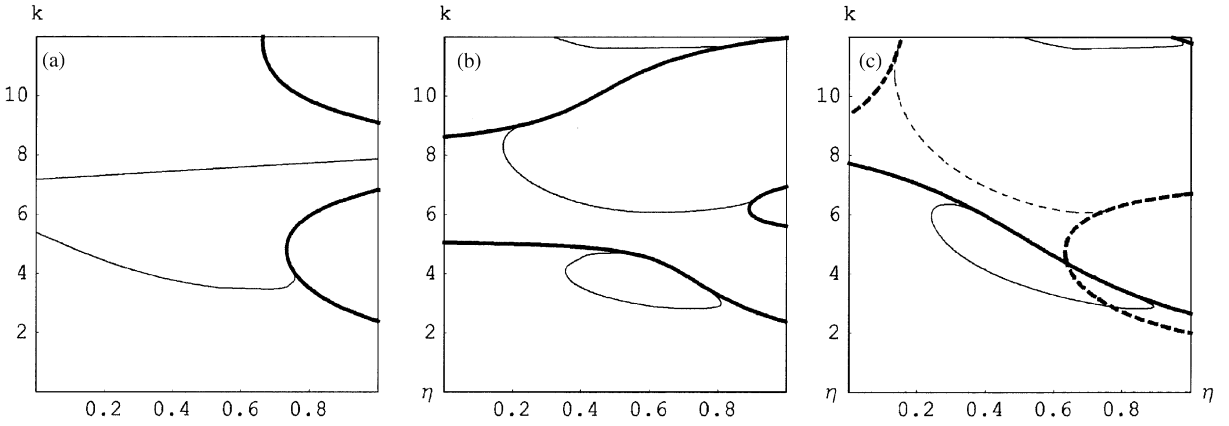

Fig. 2. Divergence and flutter critical loads for $D^* = 1$, and $\lambda = 3.5$: (a) built in; (b) simply supported; (c) free free.

anticipate that within any divergence mode (i.e. disregarding discontinuities) the divergence load will decrease as η increases: we term this behavior normal and any other behavior anomalous.

4.1.1. Built in

Fig. 2(a) shows the buckling loads for BI boundary conditions. The primary divergence curve is the heavy small arc extending from $\{\eta, k\} \approx \{1, 2.55\}$ down to $\{0.73, 5.00\}$ and back to $\{1, 6.92\}$. The primary flutter curve extends from $\{\eta, k\} \approx \{0, 5.40\}$ until it merges with the primary divergence curve at $\{0.83, 4.08\}$. For divergence it is important to note that the secondary divergence curve (the heavy line from $\{\eta, k\} \approx \{1, 9.25\}$ to $\{0.66, 12\}$) extends further left than the primary curve. In fact, a sequence of similar but higher load divergence curves exist above $k = 12$. These extend progressively further to the left and provide divergence loads for $0.5 < \eta \leqslant 1$. For flutter, it is important to note that the secondary flutter curve (the light curve from $\{\eta, k\} \approx \{0, 7.27\}$ to $\{1, 7.95\}$) provides flutter loads for any $0 \leqslant \eta \leqslant 1$. The BI plate is governed by flutter for $\eta < 0.83$ and by divergence for $\eta > 0.83$. The combined instability curve decreases as η increases except for a small anomalous region where the flutter load rises to meet the divergence load just before the transition $\eta \approx 0.83$. This is the general pattern for BI plates. The interesting question is how the critical value of η at which the transition occurs varies withaspect ratio λ and material orthotropy ratio D^*.

4.1.2. Simply supported

Fig. 2(b) shows the buckling loads for SS boundary conditions. The primary divergence curve extends completely across the figure from $\eta = 0$ and $k \approx 5.15$ to $\eta = 1$ and $k \approx 2.48$. The primary flutter curve is the isolated loop below the primary divergence curve extending from $\{\eta, k\} \approx \{0.35, 4.19\}$ to $\{\eta, k\} \approx \{0.81, 2.96\}$. For flutter it is important to note that the secondary flutter curves extends further right and left than the primary flutter curve. The SS plate is governed by a divergence mode for $0 \leqslant \eta < 0.35$, which jumps down to a flutter mode at $\eta \approx 0.35$, and jumps back up to a divergence mode at $\eta \approx 0.81$. The resulting stability curve decreases as η increases except for the jump discontinuity at $\eta \approx 0.81$ and a small anomalous region below the jump. This is the general pattern for SS plates. The interesting question is how the critical η values ($\eta \approx 0.35$ and $\eta \approx 0.81$ for $D^* = 1.0$ and $\lambda = 3.5$) vary with material orthotropy ratio D^* and aspect ratio λ.

4.1.3. Free free

The analysis of the FF boundary condition is more involved since in this case the instability can have either odd (OFF) or even (EFF) mode shape.

Fig. 2(c) combines the flutter and divergence stability curves for the OFF and EFF modes. As before, the heavy curves are divergence loads while the light curves are flutter loads. The solid curves are even EFF loads the dashed curves are odd OFF loads. The FF plate is governed by an even divergence mode for $0 \leqslant \eta < 0.24$, which jumps down to an even flutter mode for $0.24 < \eta < 0.77$ and is followed by a continuous transition to an odd divergence mode for $0.77 < \eta \leqslant 1$. This is the general behaviour for FF plates. The question of interest is how the stability intervals change with aspect ratio λ and material orthotropy D^*.

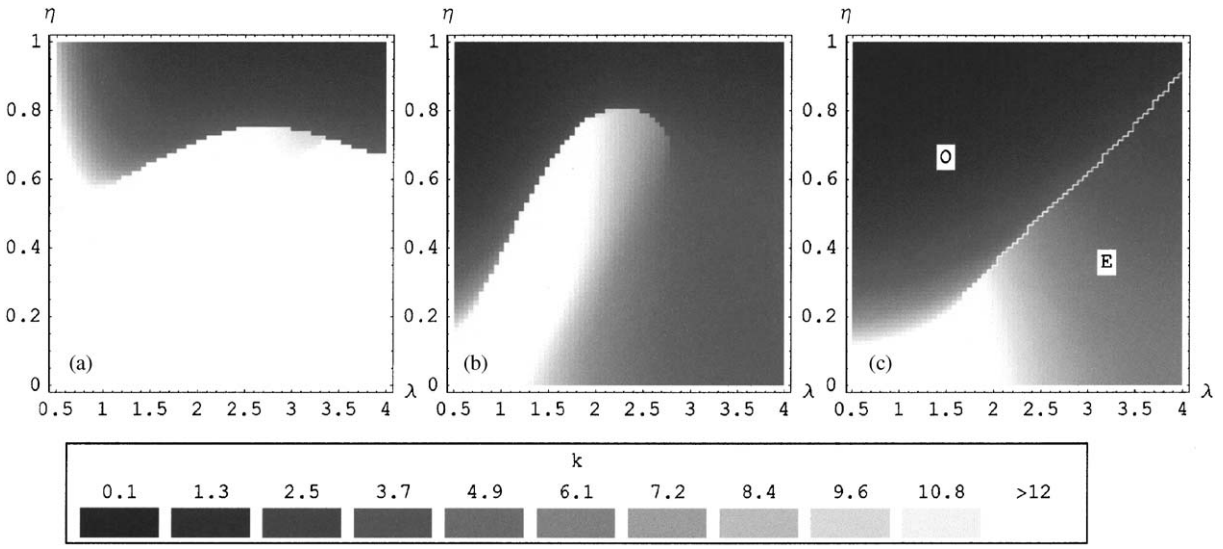

Fig. 3. Divergence critical loads for $D^* = 1$: (a) built in; (b) simply supported; (c) free free.

4.2. Divergence load dependence on aspect ratio λ

Having established the characteristic behavior of the different boundary conditions by examining $\lambda = 3.5$, we now proceed to examine the effect on the divergence load of changing the aspect ratio λ. Fig. 3 shows the dependence of divergence critical loads for $0 \leqslant \eta \leqslant 1$ and $0.5 \leqslant \lambda \leqslant 4$ when $D^* = 1.0$. The data for each boundary condition (BI, SS, and FF) was compiled as described in the computational notes to give the data sets shown in Fig. 3. Blank regions in Fig. 3 indicate either that no divergence load exists or that the non-dimensional load exceeds 12. We anticipate that within any divergence mode (i.e. disregarding discontinuities) the divergence load will decrease as both λ and η increase: we term this behavior normal and any other behavior anomalous.

4.2.1. Built in

Fig. 3(a) shows the divergence loads less than 12 for a BI plate with $D^* = 1$. The region at the top of the figure is the fundamental divergence region. Lower resolution computations with higher maximum k values show that: the small island of divergence critical loads below the fundamental divergence region is the first of several higher order divergence loads; that these loads completely fill the region $\eta > 0.5$; and there are no divergence critical loads for the BI plate with $\eta < 0.5$. The divergence critical load is normal throughout the entire region.

4.2.2. Simply supported

Fig. 3(b) shows the divergence critical loads less than 12 for a SS plate with $D^* = 1$. Lower resolution computations with higher maximum k values show that in contrast to the BI case for the SS plate there are divergence critical loads for any $0 \leqslant \eta \leqslant 1$ and $0.5 < \lambda < 4$. The divergence load is normal except for the strongly anomalous region in the lower left hand corner (where the

divergence critical load increases as λ increases) in advance of the discontinuity along the curve from $\{\lambda, \eta\} \approx \{0.5, 0.19\}$ to $\{2.23, 0.81\}$ and a very slight increase in the divergence load with λ in the upper right hand corner.

4.2.3. Free free

As before, the analysis of the FF boundary condition is more involved since for a given λ and η the lower of the OFF and EFF divergence loads provides the governing FF divergence load.

Fig. 3(c) combines the OFF and EFF divergence data to show the dependence of the FF divergence load on λ and η. An "O" or "E" indicates an Odd or Even mode shape. The load is normal throughout the entire region.

4.3. Flutter load dependence on aspect ratio λ

Having characterized the divergence loads associated with each boundary condition, we now proceed to examine the effect on the flutter load of changing the aspect ratio λ and follower load η. Fig. 4 shows the non-dimensional flutter loads for $0 \leqslant \eta \leqslant 1$ and $0.5 \leqslant \lambda \leqslant 4$ when $D^* = 1.0$. The data for each boundary condition (BI, SS, and FF) was compiled as described in the computational notes to give the data sets shown in Fig. 4. Blank regions in Fig. 4 indicate that either no flutter load exists, that the non-dimensional load exceeds 12, or the non-dimensional frequency exceeds 10. We anticipate that within any flutter mode (i.e. disregarding discontinuities) the flutter load will decrease with both λ and η: we term this behavior normal and any other behavior anomalous.

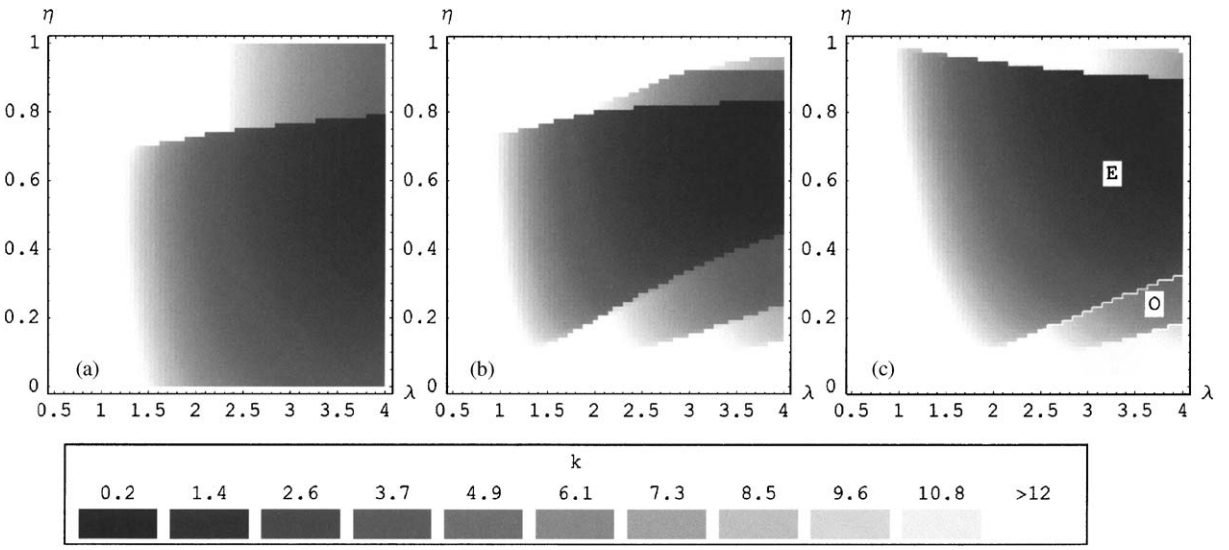

Fig. 4. Flutter critical loads for $D^* = 1$: (a) built in; (b) simply supported; (c) free free.

4.3.1. Built in

Fig. 4(a) shows the flutter loads for a BI plate with $D^* = 1$. The large lower region is the fundamental flutter region; the small upper region is a higher order flutter load. Lower resolution computations with higher maximum k values show that both regions expand to the left to provide flutter loads for $0 \leqslant \eta \leqslant 1$ and $0.5 < \lambda < 4$. The flutter load is normal throughout the entire region.

4.3.2. Simply supported

Fig. 4(b) shows the flutter loads for a SS plate with $D^* = 1$. The central fundamental flutter region is flanked (above and below) by a higher order flutter mode which is in turn flanked (above and below) by another higher order flutter mode. Lower resolution computations with higher maximum k values show that these and additional higher order flutter modes expand to the left to provide flutter loads for $0 \leqslant \eta \leqslant 1$ and $0.5 < \lambda < 4$. The flutter load is normal except for a very small, slightly anomalous region for large λ near the top of the primary flutter curve around $\eta \approx 0.8$.

4.3.3. Free free

As before, the analysis of the free boundary condition is more involved since for a given λ and η the lower of the OFF and EFF flutter loads provides the governing FF flutter load.

Fig. 4(c) combines the OFF and EFF flutter data to show the dependence of the FF flutter load on λ and η. An "O" or "E" indicates an Odd or Even mode shape. The load is normal throughout the entire region.

4.4. Stability regions in the λ–η plane

For a given λ and η the lower of the divergence and flutter loads determines the stability regions shown in Fig. 5. In Fig. 5, "D" and "F" indicate if Divergence or Flutter provides the governing instability in that region.

4.4.1. Built in

Fig. 5(a) combines the divergence and flutter data (Figs. 3(a) and 4(a)) to show the stability regions for the BI plate (with $D^* = 1.0$) in the λ–η plane. The boundary between the "D" and "F" regions shows how the critical value of η in Fig. 2(a) varies with λ.

4.4.2. Simply supported

Fig. 5(b) combines the divergence and flutter data (Figs. 3(b) and 4(b)) to show the stability regions for the SS plate (with $D^* = 1.0$) in the λ–η plane. The top and bottom boundaries of the central "F" region shows how the central flutter loop (discussed in Fig. 2(b) for $\lambda = 3.5$) varies with λ.

4.4.3. Free free

Fig. 5(c) combines the divergence and flutter data (Figs. 3(c) and 4(c)) to show the stability regions for the FF plate (with $D^* = 1.0$) in the λ–η plane. In Fig. 5(c), "E" and "O" indicate if the Even or Odd mode provides the governing instability. The lower and upper boundaries of the central "EF" region show how the lower end of the EFF flutter loop and intersection of the EFF flutter and OFF divergence curves (discussed in Fig. 2(c) for $\lambda = 3.5$) varies with λ.

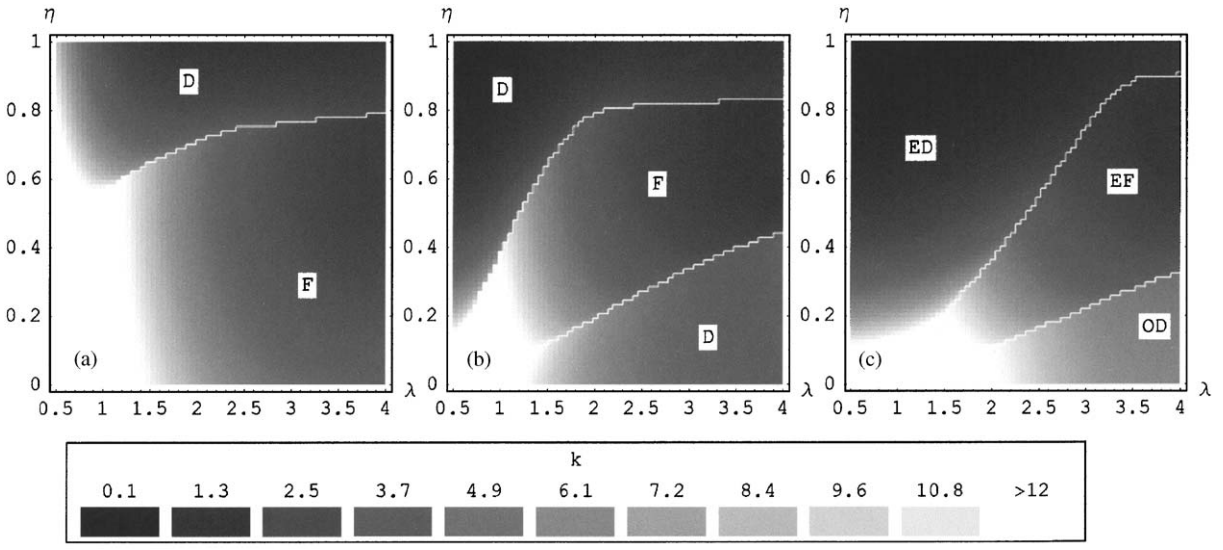

Fig. 5. Divergence/flutter critical loads for $D^* = 1$: (a) built in; (b) simply supported; (c) free free.

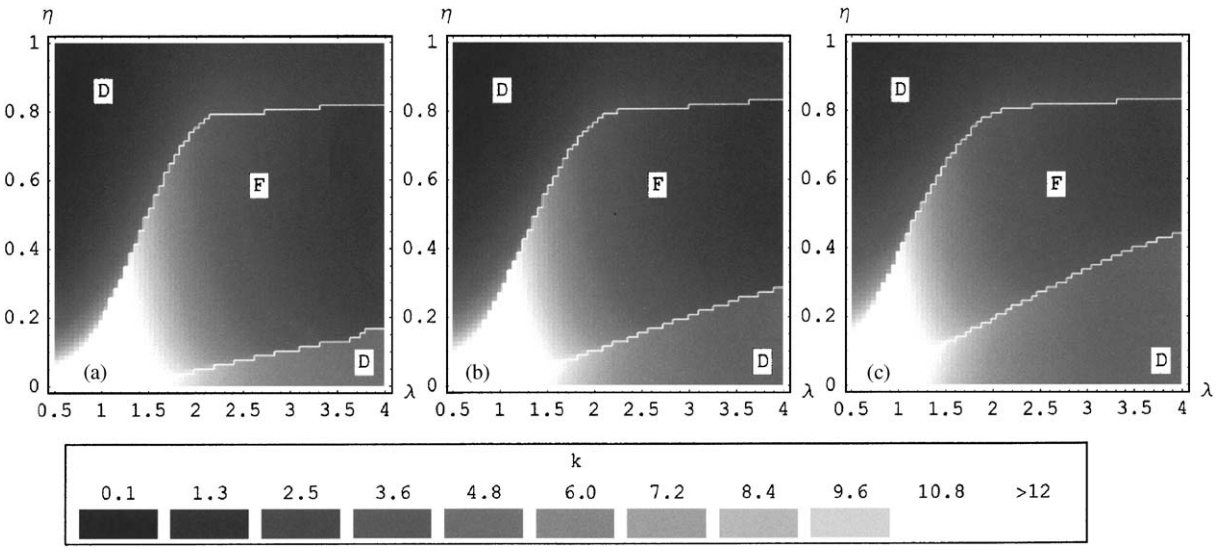

Fig. 6. Simply supported divergence/flutter critical loads: (a) $D^* = 0.25$; (b) $D^* = 0.5$; (c) $D^* = 1.0$.

4.5. Divergence and flutter load dependence on D^*

Fig. 6 shows the variation of the stability regions for a SS plate with D^*. Comparing Fig. 6(a) showing $D^* = 0.25$, Fig. 6(b) showing $D^* = 0.5$, and Fig. 6(c) showing $D^* = 1.0$ shows the two primary effects of varying D^*: (1) divergence and flutter loads increase with D^* as expected; (2) the range of η values where the flutter instability governs decreases with D^*.

We conclude by noting that similar effects are observed for the other boundary conditions.

5. Conclusions

This computational study analyzes flutter and divergence instabilities of rectangular, specially orthotropic plates subject to subtangential loading. Particular attention is paid to dependence of the buckling mode (divergence or flutter) and buckling load on the degree to which the loading is subtangential. From a design perspective, the significant conclusion is that the physically important buckling mode can jump from divergence to flutter and back as the loading changes from conservative to follower.

Specifically, the paper examines buckling mode and buckling load dependence on: tangential follower parameter, η; aspect ratio, λ; material orthotropy parameter, D^*; and boundary condition (built in, simply supported, and free free). The primary conclusions are:

(1) For given aspect ratio λ and orthotropy coefficient $D^* = 1$ the range $0 \leqslant \eta \leqslant 1$ for the follower parameter is divided into intervals corresponding to different governing instabilities. The number and size of the intervals as well as the corresponding instability is strongly affected by the boundary condition. The configuration of the intervals is independent of the aspect ratio, λ. The aspect ratio affects the magnitude of the buckling load and the location of the boundaries between the stability intervals.

(2) For fixed orthotropy coefficient, D^*, the λ–η plane is divided into stability regions with different governing instabilities. The number and size of the regions as well as the corresponding instability is strongly affected by the boundary condition.

(3) For a given boundary condition the configuration of the stability regions is independent of the orthotropy coefficient, D^*. The orthotropy coefficient affects only the magnitude of the buckling load and the size of the stability regions.

References

[1] W.H. Wittrick, Correlation between some stability problems for orthotropic and isotropic plates under biaxial and uniaxial direct stress, *The Aeronautical Quarterly* IV (1952) 83–92.
[2] P. Shulesko, A reduction method for buckling problems of orthotropic plates, *The Aeronautical Quarterly* I (1956) 145–155.
[3] E.J. Brunelle, G.A. Oyibo, Generic buckling curves for specially orthotropic rectangular plates, *AIAA Journal* 12 (8) (1982) 1150–1156.
[4] I.A. Veres, L.P. Kollar, Buckling of orthotropic plates subjected to biaxial normal forces, *Journal of Composite Materials* 35 (7) (2001) 625–635.
[5] C.J. Brown, A.L. Yettram, Elastic stability of orthotropic plates using the conjugate load/displacement method, *Computers and Structures* 53 (6) (1994) 1493–1496.
[6] K.L. Kyu, Buckling analysis of orthotropic plates using a finite element method of assumed displacement functions, *Computers and Structures* 42 (2) (1992) 159–166.
[7] I.E. Harrik, R. Ekambaram, Elastic stability of orthotropic plates, *Thin-Walled Structures* 6 (1988) 405–416.
[8] T.K. Tung, J. Surdenas, Buckling of orthotropic plates under biaxial loading, *Journal of Composite Materials* 21 (1987) 124–128.

[9] C. Libove, Buckle pattern of biaxially compressed simply supported orthotropic rectangular plates, *Journal of Composite Materials* 17 (1983) 45–48.
[10] P.M. Culkowski, H. Reismann, Plate buckling due to follower edge forces, *Journal of Applied Mechanics* 99 (1977) 768–769.
[11] H.H.E. Leipholz, Stability of a rectangular simply supported plate subjected to nonincreasing tangential follower forces, *Journal of Applied Mechanics* 45 (1978) 223–224.
[12] H.H.E. Leipholz, F. Pfendt, On the stability of rectangular completely supported plates with uncoupled boundary conditions subjected to uniformly distributed follower forces, *Computer Methods in Applied Mechanics and Engineering* 30 (1982) 19–52.
[13] H.H.E. Leipholz, F. Pfendt, Application of extended equations of Galerkin to stability problems of rectangular plates with free edges and subjected to uniformly distributed follower forces, *Computer Methods in Applied Mechanics and Engineering* 37 (1983) 341–365.
[14] S. Adali, Stability of a rectangular plate under nonconservative and conservative forces, *International Journal of Solids and Structures* 18 (12) (1982) 1043–1052.
[15] A. Kumar, A.K. Srivasta, Stability of thin rectangular elastic plates under a follower force, *Mechanics Research Communications* 13 (3) (1986) 165–168.
[16] K. Higuchi, E.H. Dowell, Effects of the Poisson ratio and negative thrust on the dynamic stability of a free plate subjected to a follower force, *Journal of Sound and Vibration* 129 (2) (1989) 255–269.
[17] E. Reissner, F.Y.M. Wan, A follower load buckling problem for rectangular plates, *Journal of applied mechanics* 59 (1992) 674–676.
[18] Q.H. Zuo, H.L. Shreyer, Flutter and divergence instability of nonconservative beams and plates, *International Journal of Solids and Structures* 33 (9) (1996) 1355–1367.
[19] M. Farshad, Stability of a cantilever plates subjected to biaxial subtangential loading, *Journal of Sound and Vibration* 58 (4) (1978) 555–561.
[20] J.H. Kim, H.S. Kim, A study on the dynamic stability of plates under a follower load, *Computers and Structures* 74 (2000) 351–363.